

X-Ray Determination of Electron Momenta in Li, Be, B, Na, Mg, Al, and LiF

WALTER C. PHILLIPS

Electronics Research Center, National Aeronautics and Space Administration, Cambridge, Massachusetts

AND

R. J. WEISS

Army Materials and Mechanics Research Center, Watertown, Massachusetts

(Received 13 February 1968)

Details of the ground-state electron momentum density in Li, Be, B, LiF, Na, Mg, and Al have been investigated by means of high-resolution Compton line-shape measurements. A sharp discontinuity is observed in the momentum density near the Fermi Surface in Li, Na, Mg, and Al, whereas in Be the discontinuity (if any) is too small to be discerned. Above the Fermi momentum, these metals all exhibit high-momentum tails in their valence-electron momentum densities which can be attributed largely to electron-electron correlations. The momentum density in Be and Al is sensitive to crystallographic orientation, while the density measured in Li and Na is essentially spherically symmetric. In both Be and B the measured valence-electron densities are more $2p$ -like than $2s$ -like. The measured momentum density of LiF resembles a superposition of calculated free-atom Li^+ and F^- , rather than Li^0 and F^0 momentum densities. Agreement between the data, analyzed in the impulse approximation, and Hartree-Fock calculations for the core-electron momentum densities is good in Li, B, Na, and Mg, but unsatisfactory in Be and Al.

INTRODUCTION

IT has been known for over forty years that the ground-state linear momentum distribution of electrons in solids can be investigated by measurements of Compton x-ray scattering.¹ Yet only recently have such experiments been carried out with sufficient accuracy to allow observation of interesting features of the momentum distributions.² Unlike x-ray scattering-factor measurements, which are insensitive to the outer-electron charge density and are encumbered by problems of extinction and absolute values, the Compton measurements are both sensitive to and quite simply related to the momentum distribution of the outer electrons. Thus the Compton-scattering experiments can provide a critical test of band calculations (especially when correlation effects are included).

For many years, the angular correlation of positron annihilation radiation has been used to determine the momentum distribution of the outer electrons in solids. In order to obtain the electron momentum distribution from such measurements, it is necessary to (1) know the positron wave function in the solid and (2) assume negligible perturbation of the annihilating electron by the positron. Since no such problems arise in Compton scattering, a comparison of Compton x-ray and positron experimental results provides direct information about (1) and (2) (both of which have also been examined theoretically).³ The outer-electron momentum distributions determined from the present x-ray results and from previous positron results exhibit both similarities and differences, suggesting that these two techniques may be complementary.

The experimental work reported here is of Compton line-profile measurements on Li, Be, B, LiF, Na, Mg,

and Al. The results presented indicate the detail presently attainable with a slightly modified commercial x-ray spectrograph. Although the resolution provided by this apparatus is better than that employed in previous Compton line-profile investigations, still higher resolution can be achieved with a more specialized instrument.

THEORY

The theory of the Compton line shape has been given by several authors.⁴ Platzman and Tzoar, by considering time-dependent scattering theory, justify the use of the impulse approximation.⁵ The impulse approximation is valid if (1) the photon interacts with only a single electron and (2) the binding forces between the ejected electron and the other particles in the system are essentially constant during the time of the collision. If the incoming-photon energy is large compared with the energies of the electrons in the system, condition (1) is satisfied. Furthermore, if the final energy of the Compton electron is much greater than its initial energy, the collision time will be much shorter than the time required for any rearrangement of the remaining electrons, and condition (2) will be satisfied. The net effect is that the photon and electron exchange energy and momenta in a constant potential field.

In the impulse approximation the Compton cross section for an electron scattered into a plane-wave state with momentum \mathbf{p} is given by

$$\frac{d\sigma}{dk} \propto \sum_{\mathbf{p}} \left| \int d^3r e^{i\mathbf{p}\cdot\mathbf{r}} e^{i(\mathbf{k}-\mathbf{k}_0)\cdot\mathbf{r}} \varphi(\mathbf{r}) \right|^2 \delta(E(p) - E(p_0) - \Delta E_\gamma) \\ \propto \sum_{\mathbf{p}} |\chi(\mathbf{p} + \mathbf{k} - \mathbf{k}_0)|^2 \delta(E(p) - E(p_0) - \Delta E_\gamma) \quad (1)$$

¹ For a review of early work, see A. H. Compton and S. K. Allison, *X-Rays in Theory and Experiment* (D. Van Nostrand, Inc., Princeton, N. J., 1967), 2nd ed.

² M. Cooper and J. A. Leake, *Phil. Mag.* **15**, 1201 (1967).

³ J. Melngailis and S. DeBenedetti, *Phys. Rev.* **145**, 400 (1966); J. P. Carbotte and S. Kahana, *ibid.* **139**, A213 (1965).

⁴ W. E. Duncanson and C. A. Coulson, *Proc. Phys. Soc. (London)* **57**, 190 (1945); G. E. Kilby, *ibid.* **86**, 1037 (1965); P. M. Platzman and N. Tzoar, *Phys. Rev.* **139**, A410 (1965).

⁵ G. F. Chew and G. C. Wick, *Phys. Rev.* **83**, 636 (1952).

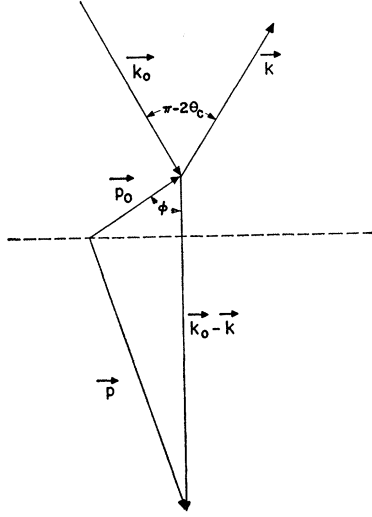


FIG. 1. Diagram of the Compton process in a plane in momentum space.

(using atomic units). The final and initial photon momenta are \mathbf{k} and \mathbf{k}_0 , the electron initial momentum and energy are \mathbf{p}_0 and $E(p_0)$, $\varphi(\mathbf{r})$ is the ground-state one-electron wave function of the electron before it is ejected, $\Delta E_\gamma = h(\nu_0 - \nu)$ is the energy loss of the photon, and the δ function signifies conservation of energy. $\chi(\xi)$ is the momentum eigenfunction, i.e., the momentum transform of $\varphi(\mathbf{r})$:

$$\chi(\xi) = (2\pi)^{-3/2} \int d^3r e^{-i\xi \cdot \mathbf{r}} \varphi(\mathbf{r}). \quad (2)$$

The factor $(2\pi)^{-3/2}$ ensures normalization of χ in momentum space when φ is normalized in configuration space.

Referring to Fig. 1, conservation of momentum and energy yield respectively

$$\begin{aligned} p^2 &= p_0^2 + |\mathbf{k} - \mathbf{k}_0|^2 - 2p_0 \cos\phi |\mathbf{k} - \mathbf{k}_0|, \\ p^2 &= p_0^2 + 2mh\Delta\nu. \end{aligned} \quad (3)$$

Therefore,

$$\begin{aligned} p_0 \cos\phi &= \frac{|\mathbf{k} - \mathbf{k}_0|}{2} - \frac{mh\Delta\nu}{|\mathbf{k} - \mathbf{k}_0|} \equiv -z, \\ z &\equiv mc \frac{h\nu_0 \sin\theta_c}{mc^2} \\ &\times \left\{ \frac{mc^2 \Delta\nu / \nu_0}{2h\nu_0 \sin^2\theta_c [1 - \Delta\nu/\nu_0 + (\Delta\nu/\nu_0)^2 (1/4 \sin^2\theta_c)]^{1/2}} \right. \\ &\quad \left. - \left[1 - \frac{\Delta\nu}{\nu_0} + \left(\frac{\Delta\nu}{\nu_0} \right)^2 \frac{1}{4 \sin^2\theta_c} \right]^{1/2} \right\}. \end{aligned}$$

Thus, if \mathbf{k} and \mathbf{k}_0 are fixed experimentally, $p_0 \cos\phi$ is uniquely determined, and the summation over final states \mathbf{p} becomes essentially an integration over a plane

in momentum space normal to the scattering vector $\mathbf{k} - \mathbf{k}_0$ and at a distance $p_0 \cos\phi$ from the origin.

For a one-electron wave function separable into angular and radial parts [$\varphi(\mathbf{r}) = \Theta(\theta)\Phi(\phi)R(r)$], where the angular functions are the hydrogenic one-electron solutions], it can be shown that

$$\chi_n(\mathbf{p}_0) = \left(\frac{2}{\pi} \right)^{1/2} \Theta(\theta')\Phi(\phi') \int R(r) j_n(p_0 r) r^2 dr, \quad (4)$$

where θ' and ϕ' are the corresponding angular variables in momentum space and the subscript n denotes the one-electron orbital quantum number (0, 1, 2, 3 for s, p, d, f , respectively). If we are dealing with s electrons or make measurements which average over the angular variables, integration over the plane in momentum space gives for Eq. (1)

$$\frac{d\sigma}{dk} \propto 2\pi \int_{|\mathbf{z}|} |\chi(p_0)|^2 p_0 dp_0 \equiv J(z), \quad (5)$$

where

$$|\chi(p_0)|^2 = \frac{2}{\pi} \left[\int R(r) j_n(p_0 r) r^2 dr \right]^2. \quad (6)$$

Calculated values of the Compton line shape $J(z)$ for Hartree-Fock free-atom one-electron functions have been calculated using Clementi wave functions.⁶ These calculated $J(z)$ functions will be used in describing the results reported here. It is convenient to introduce a parameter q which has the dimensions of momentum and is proportional to the wavelength separation l from the center of the Compton line for an unbound electron:

$$\begin{aligned} q &\equiv mc \frac{l}{2\lambda_0 \sin\theta_c}, \\ l &= \lambda - \left(\lambda_0 - \frac{2h \sin^2\theta_c}{mc} \right), \quad \frac{2h}{mc} = 0.04852 \text{ \AA}, \end{aligned} \quad (7)$$

where $2\theta_c$ is the Compton scattering angle, λ_0 is the incident wavelength, and λ is the final wavelength. For conditions ordinarily met in practice ($\theta_c \gtrsim 60^\circ$, $\lambda_0 \sim 0.7 \text{ \AA}$), $z \cong q$. Some values of z as a function of q for Mo $K\alpha$ radiation ($\lambda_0 = 0.71$) and for several values of θ_c are given in Table I. The differences ($z - q$) are of the order of a few percent.

Equation (5) is the fundamental working equation for Compton line-shape measurements of polycrystalline samples in the impulse approximation, assuming that the electrons are described by free-atom wave functions. From a measurement of $J(z)$ one can obtain $|\chi(p_0)|^2$ by inversion, i.e.,

$$|\chi(p_0)|^2 = \left| \frac{1}{2\pi z} \frac{dJ}{dz} \right|, \quad (8)$$

$$4\pi |\chi(p_0)|^2 p_0^2 \equiv I(p_0) = \left| 2z \frac{dJ}{dz} \right|,$$

⁶ R. J. Weiss, W. C. Phillips, and A. Harvey, *Phil. Mag.* **17**, 146 (1968).

TABLE I. Values of z versus q for Mo $K\alpha$ radiation ($\lambda=0.71 \text{ \AA}$) for three values of the Compton scattering angle θ_c .

q (a.u.)	z (a.u.)		
	$\theta_c=45^\circ$	$\theta_c=75^\circ$	$\theta_c=90^\circ$
-4.0	-4.01	-3.99	-3.98
-3.5	-3.50	-3.48	-3.47
-3.0	-3.00	-2.97	-2.96
-2.5	-2.49	-2.47	-2.46
-2.0	-1.99	-1.97	-1.96
-1.5	-1.49	-1.47	-1.47
-1.0	-0.99	-0.98	-0.98
-0.5	-0.49	-0.49	-0.49
0.0	0.00	0.00	0.00
0.5	0.49	0.48	0.48
1.0	0.98	0.96	0.95
1.5	1.46	1.43	1.43
2.0	1.94	1.90	1.90
2.5	2.42	2.37	2.36
3.0	2.90	2.84	2.83
3.5	3.37	3.30	3.29
4.0	3.84	3.76	3.75
4.5	4.31	4.21	4.20
5.0	4.78	4.67	4.65
5.5	5.24	5.12	5.10
6.0	5.71	5.56	5.54
6.5	6.16	6.01	5.98
7.0	6.62	6.45	6.42
7.5	7.08	6.89	6.86
8.0	7.53	7.32	7.29
8.5	7.98	7.75	7.72

where $I(p_0)$ is the linear momentum density between p_0 and p_0+dp_0 . Furthermore, since $|\chi(p_0)|^2$ gives the probability per unit volume in momentum space of finding an electron with linear momentum p_0 , one can also obtain the expectation value of the kinetic energy:

$$\langle KE \rangle = 2\pi \int_0^\infty |\chi(p_0)|^2 p_0^4 dp_0 \quad (\text{atomic units}). \quad (9)$$

Under conditions of very large energy transfer (compared with the binding energy), there is also the condition that

$$\int_{-\infty}^\infty J(z) dz \cong 1 - f^2(\sin\theta_c/\lambda_0) \quad (10)$$

per electron, where f is the x-ray scattering factor.

For a many-electron atom, the Compton cross section is a sum of the contributions from each electron. In dealing with aspherical momentum densities, Eqs. (5)–(9) must be modified. In this case, Eq. (5) involves the momentum distribution in a plane normal to the x-ray scattering vector and at a distance $|z|$ from the origin.

The discussion above has been limited to free atoms. For electrons in a crystal lattice, Berko and Plaskett have shown that for Bloch electrons with wave function $\psi_\kappa(\mathbf{r})$, $|\chi_{\text{sol}}(\mathbf{p}_0)|^2$ involves a sum of contributions $|\chi_\kappa(\mathbf{p}_0)|^2$ from all Bloch electrons whose wave vector κ either equals \mathbf{p}_0 or differs from \mathbf{p}_0 by a reciprocal lattice vector.⁷

⁷ S. Berko and J. S. Plaskett, Phys. Rev. **112**, 1877 (1958).

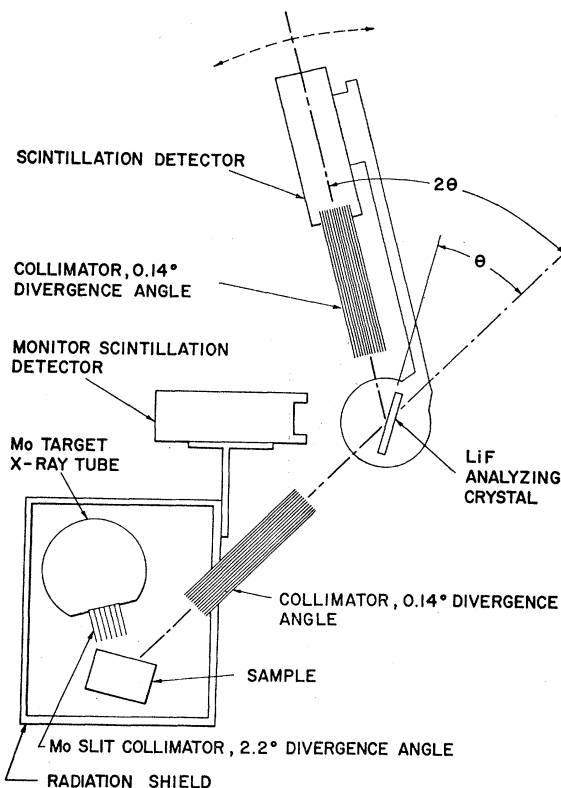


FIG. 2. Schematic drawing of the apparatus. The angle between extreme rays defines the collimator divergence angle.

EXPERIMENTAL DETAILS

The basic technique for obtaining our Compton profiles has been used previously.⁸ Figure 2 shows a schematic diagram of our apparatus, a modified Norelco spectrograph. A molybdenum-target x-ray tube operating at approximately 50 kV (full-wave rectified) and 50 mA was employed. Molybdenum Soller slits fixed to the x-ray-tube window reduce the divergence of the beam striking the sample to 2.2°. (Divergences are taken as the angle between the extreme rays.) X rays scattered by the sample through $\sim 117^\circ$ are collimated by a second set of Soller slits (divergence 0.14°), then diffracted by a LiF analyzing crystal (in symmetric reflection), and lastly collimated by a third set of Soller slits (divergence 0.14°) fixed to the NaI detector. In conjunction with the detector amplifier, a pulse-height analyzer is used to reject pulses with wavelengths far from the Mo $K\alpha$ line ($\lambda \sim 0.7 \text{ \AA}$). The x-ray-tube output is monitored by a second NaI detector and pulse-height analyzer which samples a broad beam of x rays ($\lambda \sim 0.7 \text{ \AA}$) scattered from the LiF analyzer through $\sim 80^\circ$ to 140° (see Fig. 2). A Zr filter further enhances the 0.7 \AA monitor signal. Data are obtained by accumulating counts at a fixed detector angle 2θ (analyz-

⁸ M. Cooper, J. A. Leake, and R. J. Weiss, Phil. Mag. **12**, 797 (1965).

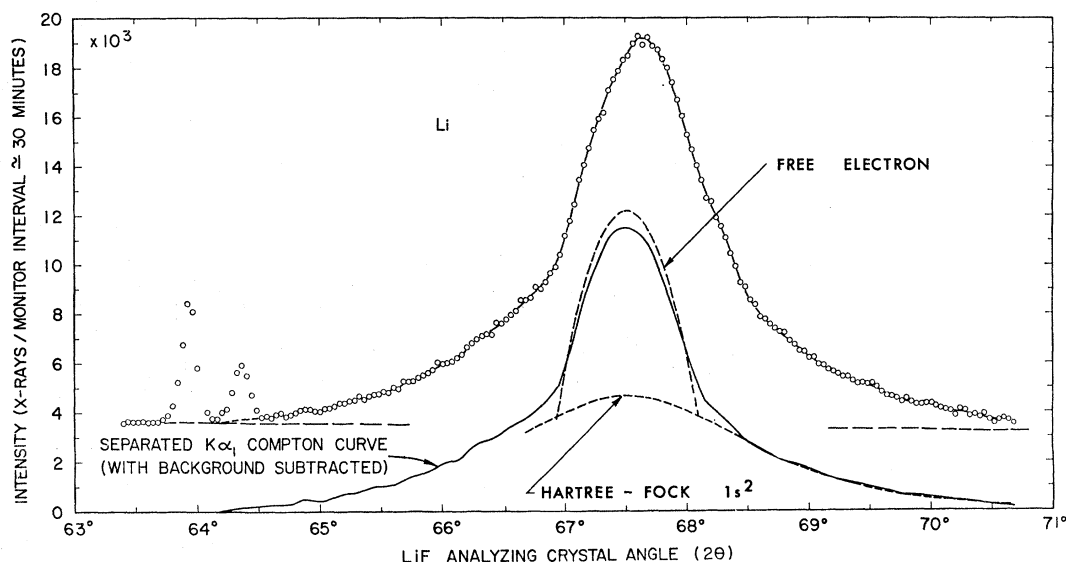


FIG. 3. Compton line for polycrystalline Li (upper curve). The lower solid curve is the separated $K\alpha_1$ component with background subtracted (and corrected for absorption). The dashed curves show (1) the calculated Hartree-Fock $1s^2$ core and (2) an inverted parabola (free-electron theory) centered at $q=0$. The total area under the two calculated curves is equal to the area under the experimental $K\alpha_1$ curve, and their area ratio satisfies Eq. (10).

ing-crystal angle θ) for a predetermined number of monitor counts.

The main effort in these measurements was to achieve higher resolution in momentum (q) space than had been previously achieved. This was accomplished by using the three sets of Soller slits and a LiF analyzing crystal with a rocking curve width of 0.1° , comparable with the divergence of the second and third sets of slits. The LiF (600) reflection was used in obtaining most of the data. When necessitated by low counting rates, the (400) reflection was employed, increasing the intensity by a factor of 3, with some loss of resolution. The geometry of the analyzing system requires that the 2θ -to- θ relationship between the detector slits and the analyzing crystal be accurately maintained. This introduces a major experimental difficulty, particularly at small 2θ , because it requires high precision in the 2-to-1 goniometer reduction gears.

The $MoK\alpha$ x rays scattered from a typical sample consist of an unmodified "elastic" component (Bragg and thermal diffuse scattering) and a broad Compton line. Similar elastic and inelastic scattering from the bremsstrahlung continuum produce a smooth background. Figure 3 shows data for polycrystalline Li. The ratio of $MoK\alpha$ Compton scattering to the continuum background at the Compton peak is 4.5. This ratio is 4.5 for Be and 1.8 for Al [for the LiF (600) reflection]. The counting rate at the Compton peak is 750 x rays per min for Be, 80 x rays per min for Al.

The intensity ratio of the α_1 to the α_2 component is 2 and the wavelength separation is 0.00429 \AA (for Mo). Thus it is straightforward to separate the α_1 component in the Compton data (after the background has been subtracted and the reflectivity of the analyzer and ab-

sorption in the sample have been accounted for), using the Rachinger method.⁹ With this procedure the short-wavelength half of the separated α_1 Compton line is more accurate, particularly where the slope is large, and therefore this side of the line was used for most of the valence-electron analysis. In obtaining the separated α_1 line, the Rachinger procedure was applied to a smooth curve drawn through the data.

Several features of the separated α_1 Compton profile for Li shown in Fig. 3 should be noted. There is a rapid change in slope at $2\theta=66.95^\circ$ and 68.14° ($z \approx \pm 0.6$) associated with the discontinuous change in momentum density at the Fermi surface. Positive and negative values of z (right and left sides of the Compton line, respectively) correspond to the ejection of an electron whose component of initial momentum along the $\mathbf{k}-\mathbf{k}_0$ direction is in the same and opposite direction, respectively, as the momentum transferred to the electron by the photon. The dashed curves indicate (1) the calculated Hartree-Fock contribution from the two core electrons ($1s^2$) and (2) an inverted parabola (free-electron theory) fitted to the valence-electron contribution. It can be seen that the valence-electron contribution has a "tail" extending beyond the discontinuity at the Fermi momentum. These higher-momentum components are expected in metals when electron-electron correlation effects are considered.¹⁰ Higher-momentum components are also introduced by terms in the free-electron wave function which involve finite reciprocal-lattice vectors. The latter contribution appears to be of secondary importance in the Compton data, since (1) the observed valence-electron intensity

⁹ W. A. Rachinger, J. Sci. Instr. 25, 254 (1948).

¹⁰ E. Daniel and S. H. Vosko, Phys. Rev. 120, 2041 (1960).

at high momenta does not show structure commensurate with the reciprocal lattice or any marked dependence on crystal orientation (for single-crystal samples) and (2) in Li and Na, where both positron-annihilation and Compton measurements have been made, the valence-electron intensity at high momenta is significantly larger in the Compton results.

The area under the core contribution should be nearly $\frac{2}{3}$ of the total area, since f^2 is very small for all electrons for the experimental conditions used [Eq. (10)]. The experimental core-electron curve is not symmetric about $z=0$, because of binding effects (see also Fig. 13). The binding energy of the core electrons is 55 eV.¹¹ Since the Mo $K\alpha_1$ - α_2 energy separation is 105 eV, the onset of the Compton scattering in Li occurs under the unmodified Mo $K\alpha$ doublet, prohibiting an exact determination of the Compton line shape in this region. Thus the experimental curve has been extrapolated to the background at 55 eV above the Mo $K\alpha_1$ position.

With the above values of scattering angle and incident wavelength, the energy transferred to valence electrons is between about 500 and 1100 eV. The center of the Compton line ($z=0$) corresponds to a photon energy loss of 834 eV. Thus for these electrons the use of the impulse approximation is surely justified. The energy transferred to the core electrons is greater than about 1000 eV on the long-wavelength side of the Compton peak where the core contribution was carefully analyzed, and to the extent that this energy is very much greater than the core-electron binding energy, the use of the impulse approximation is also valid.

While separation of the smooth bremsstrahlung background is straightforward, occasionally unwanted discrete lines appear in the vicinity of the Compton line. These are due to (1) Bragg scattering by a single-crystal sample, (2) fluorescence of impurities in the sample, and (3) thermal diffuse scattering of W $L\alpha$ contamination on the x-ray-tube target. Bragg scattering from a single crystal could be eliminated by a slight reorientation of the sample (Bragg scattering from polycrystalline samples was too weak to observe). The W $L\alpha$ lines, and most impurity fluorescence lines, occurred at wavelengths sufficiently removed from Mo $K\alpha$ that they could be eliminated by a combination of filters and energy discrimination.

From a measurement of the unmodified Mo $K\alpha$ lines the resolution function of the analyzing system (second and third Soller slits and LiF crystal) was determined to be essentially Gaussian with a full width at half-maximum $\Delta z=0.15$ [for the (600) reflection]. The divergence of the first Soller-slit set (2.2°) defined a resolution function with full width at half-maximum $\Delta z=0.06$, due to the shift in the Compton line as function of $2\theta_c$ [Eq. (11)]. As $2\theta_c$ approaches 180° , the initial beam divergence can be increased without loss of resolution,

¹¹ J. A. Bearden and A. F. Burr, Rev. Mod. Phys. **39**, 125 (1967).

but physical limitations of our spectrograph did not permit a scattering angle greater than $\sim 120^\circ$.

In the data the finite instrumental resolution smooths any discontinuity in slope and obscures structure wherever the true $J(z)$ is not essentially linear with z over the resolution width. In order to determine accurately the position of the Fermi momentum discontinuity and to resolve structure in $J(z)$, it is necessary to take account of the effects of the instrumental resolution. The magnitude of the statistical fluctuations in the data precludes working directly with the experimental slopes. The most successful method found for obtaining the true profile $J^*(z)$ is an iterative procedure which convolves successive trial $J^*(z)$ functions with the known instrumental-resolution function until agreement with the measured $J(z)$ is obtained. In the analysis of the valence-electron data presented below this procedure is employed.

The center of the Compton line (for the valence electrons), which corresponds to zero component of electron momentum along the scattering vector, is shifted in wavelength from the Mo $K\alpha$ by the well-known expression

$$\Delta\lambda = (h/mc)(1 - \cos 2\theta_c). \quad (11)$$

Using a single crystal as the scatterer, it is possible to obtain Bragg reflections from the continuum and determine $2\theta_c$. In this way, Eq. (11) was verified to about $\frac{1}{2}\%$.

All samples had a flat surface intercepting the entire beam and were oriented approximately perpendicular to the scattering vector, with the exception of the Be single crystal, a $\frac{3}{8}$ -in.-diam cylinder with its axis along (10 $\bar{1}$ 0), the Li single crystal, a $\frac{1}{2}$ -in.-diam cylinder with its axis along (110), and the B polycrystalline sample, which consisted of several odd-shaped pieces of grey-black crystalline B (presumably the tetragonal form). Some LiF and Al single crystals were $\frac{3}{16}$ -in. thick; the other samples were about $\frac{1}{2}$ -in. thick. No multiple scattering was observed in the data presented here. Oxidation of the Li and Na was prevented by a paraffin or oil coating thin enough that it did not give rise to appreciable scattering. All data were taken with the samples at room temperature.

RESULTS

Li and Na

As shown in Fig. 3 and discussed in the preceding section, a Hartree-Fock $1s^2$ free-atom calculation [Eq. (5)] provides a good fit to the experimental Li core at high values of momentum (z) on the long-wavelength side of the Compton line. In the region of the unmodified line (shortest wavelengths), binding becomes important and precludes the use of the impulse approximation. In Na agreement is again within the experimental error between a calculated Hartree-Fock $2s^2 2p^6$ core and the experimental $J(z)$ for large z , even on the short-wave-

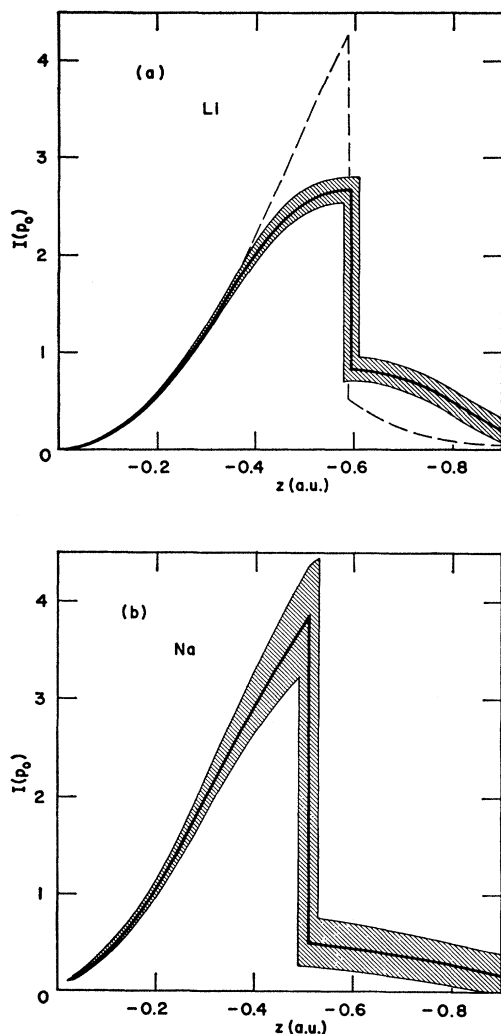


FIG. 4. Momentum density for the valence electron in (a) polycrystalline Li and (b) polycrystalline Na, obtained from the slope of the measured $K\alpha_1$ Compton line (corrected for absorption and instrumental resolution), after subtracting background and the calculated Hartree-Fock core ($1s^2$ for Li, $2s^2 2p^6$ for Na). The cross-hatched areas represent the experimental uncertainty, which arises principally from the uncertainty in determining the slope of the Compton line. The dashed curve in (a) is from Ref. 13.

length side of the Compton line. Binding appears not to affect significantly the Na line shape except in the immediate neighborhood of the unmodified line. (The binding energies for the Na core are 63 and 31 eV for the $2s$ and $2p$ electrons, respectively.¹¹ On the long-wavelength side of the Compton line the $1s$ electrons can also be excited, since the $1s$ binding energy is 1072 eV, but in the experimental profile the $1s$ electrons did not contribute a measurable intensity.) The calculated core functions, when fitted to the Li and Na data, satisfy Eq. (10) within the experimental error.

The intensity not accounted for by the calculated core $J(z)$ arises from the valence electron in Li and Na. Plotted in Fig. 4 are the valence-electron momen-

tum densities $I(p_0)$ for Li and Na, obtained from the slopes of the experimental $J(z)$ curves after correcting for instrumental resolution as explained above. The discontinuities associated with the Fermi momentum are clearly seen, as are the high-momentum tails above the Fermi momentum (p_f), which are associated with

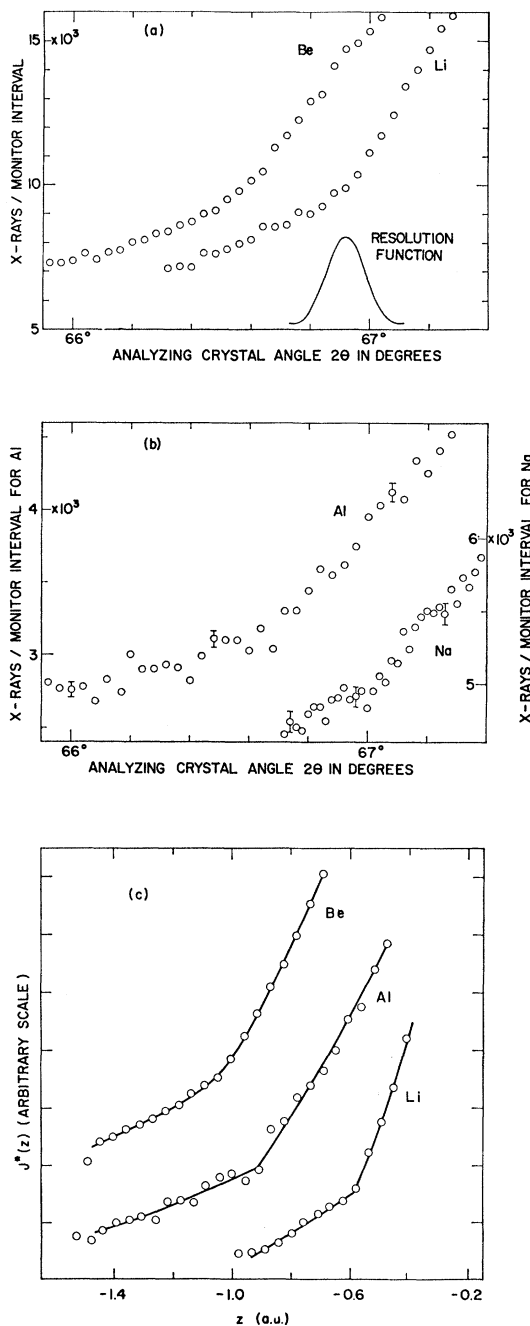


FIG. 5. Experimental Compton lines in the region of the Fermi momentum for polycrystalline (a) Li and Be and (b) Na and Al. The instrumental resolution function is shown in (a). In (c) are shown Compton lines ($K\alpha_1$ components) obtained from these data, using the iteration procedure to eliminate the broadening at p_f caused by finite instrumental resolution.

electron-electron correlation. Several experimental runs have been averaged to obtain the data represented in Fig. 4. The uncertainty in determining $I(p_0)$ is denoted by the cross-hatched region and arises principally from the uncertainty in calculating the slope of the measured $J(z)$ curve. In Fig. 5, typical data from Li, Na, and Al in the region of p_f are shown, as well as the $J^*(z)$ functions found by the iteration procedure. Also shown is the analyzer resolution function, which is given by the profile of the sharp, unmodified lines, whose known line width is about 20% of the resolution width [for the LiF (600) reflection].

The discontinuities at p_f in Fig. 4 are shown as sharp breaks because the $J^*(z)$ obtained with the above mathematical analysis appears sharp, i.e., the resolution width is sufficient to account for the observed rounding at p_f in Li and Na. The experimental values of p_f are 0.593 ± 0.015 a.u. in Li and 0.509 ± 0.02 a.u. in Na. (Significantly larger values of p_f can be arrived at when the effects of finite resolution are not considered.) The free-electron values of p_f are 0.588 a.u. for Li and 0.481 a.u. for Na. Thus p_f for Li determined from the Compton profile is in agreement with the free-electron value (agreement is also obtained in both Al and Mg), while p_f for Na is slightly larger than the free-electron value. This discrepancy is not understood.

In contrast to the Compton measurements, positron-annihilation experiments in Na and Li yield momentum distributions closer to those given by free-electron theory [$I(p_0) = 3p_0^2/p_f^3$ for $p_0 < p_f$, $I(p_0) = 0$ for $p_0 > p_f$]¹² The dashed curve in Fig. 4(a) is a calculation by Geldart, Houghton, and Vosko for an interacting electron gas with parameters appropriate to Li.¹³ The effects of correlation are obvious, although the area under the correlation tails is not so large as that found experimentally, where 14% of the total area in $I(p_0)$ for Li and Na is associated with the region above p_f . The absence of high-momentum tails (electron-electron correlation effects) in the positron measurements can be understood conceptually. The average distance between the positron and the electron with which it annihilates is of the order of the positronium Bohr radius (~ 1 Å), whereas the average distance between valence electrons in Li and Na is 3–4 Å. Thus the positron-electron pair appears partially neutral to the other electrons and electron-electron correlation effects are reduced.

The Compton profile from a Li single crystal was studied with the scattering vector along three crystallographic directions: [100], [110], and [111]. Within the experimental uncertainty of about $\pm 3\%$, no deviation from spherical symmetry in $J(z)$ was found. Positron-annihilation experiments in single-crystal Li have resolved small anisotropies.¹²

¹² J. J. Donaghy and A. T. Stewart, Phys. Rev. **164**, 391(1967); **164**, 397 (1967).

¹³ D. J. W. Geldart, A. Houghton, and S. H. Vosko, Can. J. Phys. **42**, 1938 (1964).

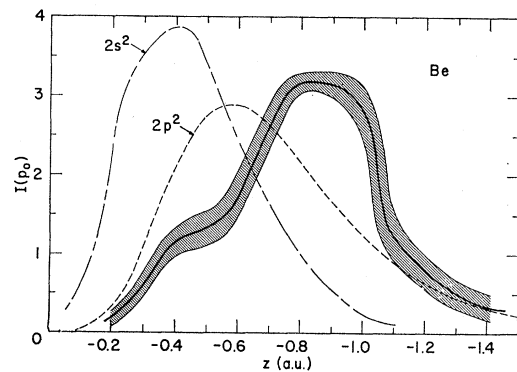


FIG. 6. Momentum density for the two valence electrons in polycrystalline Be (solid line) obtained from the slope of the $K\alpha_1$ Compton line (corrected for instrumental resolution, background, and absorption). The calculated Hartree-Fock $1s^2$ core has been subtracted from the measured Compton line to obtain the curve shown. The cross-hatched area denotes the experimental uncertainty. The dashed curves show (1) the Hartree-Fock $2s^2$ momentum density and (2) a calculated $2p^2$ momentum density, with $J(z) = (5z^2 + \gamma^2)/(z^2 + \gamma^2)^5$, $\gamma^2 = 0.672$.

Be

Large deviations from free-atom behavior are evident in single-crystal and polycrystalline Be. The experimental momentum density $I(p_0)$, corrected for instrumental resolution, for the two valence electrons in polycrystalline Be is shown in Fig. 6. This momentum density was obtained by subtracting from the data a calculated $1s^2$ contribution satisfying Eq. (10). Also shown in Fig. 6 are free-atom momentum densities for $2s^2$ and $2p^2$ configurations. [For $2p^2$, $J(z) = (5z^2 + \gamma^2)/(z^2 + \gamma^2)^5$ ($\gamma^2 = 0.672$) was used to calculate $I(p_0)$.] The data support the expectation that in the metal there is considerable promotion of the free-atom closed-shell $2s^2$ electrons to $2p$ -like states.

A discontinuous change in the slope of $J^*(z)$ was not observed in Be, in contrast to Li, Na, and Al, as shown in Fig. 5. However, in both single-crystal and polycrystalline Be the maximum curvature in the Compton line occurs at $p = 1.05 \pm 0.025$ a.u. The free-electron Fermi momentum is $p_f = 1.027$ a.u. Thus the point of maximum curvature can be associated with the location of the Fermi momentum. While current band calculations are unable to account for the high-momentum tails because they do not include correlation, the calculations of Loucks and Cutler and of Herring and Hill exhibit a considerable reduction in the density of states near the Fermi surface [compared with the parabolic free-electron $I(p_0)$].¹⁴ Such a reduction would reduce the magnitude of the discontinuity in $I(p_0)$, consistent with our observation. Also, a reduction in the density of states near the Fermi surface associated with a nearly complete p character would explain the failure to observe a significant Knight shift in Be NMR measurements.

¹⁴ T. L. Loucks and P. H. Cutler, Phys. Rev. **133**, A819 (1964); C. Herring and A. G. Hill, *ibid.* **58**, 132 (1940).

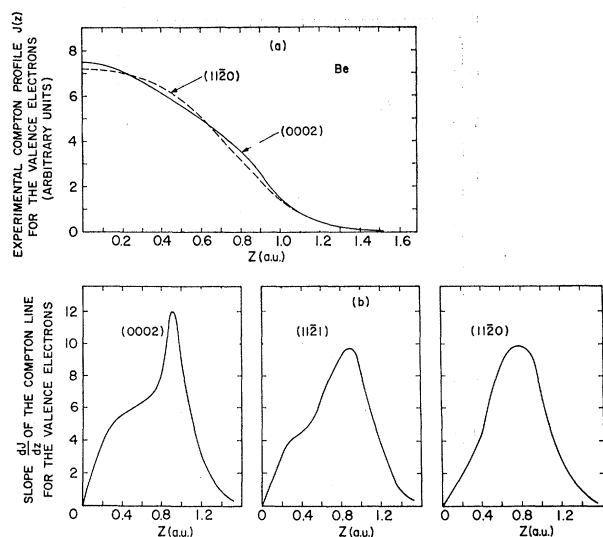


FIG. 7. (a) Long-wavelength half of the measured valence-electron Compton line ($K\alpha_1$ component) for single-crystal Be with the scattering vector in two crystallographic directions. The calculated $1s^2$ Hartree-Fock contribution and background have been subtracted from the data. The effects of instrumental resolution have not been removed. (b) Slopes of the curves shown in (a), and of a similar curve for the (1121) direction. The magnitude of the experimental uncertainty (not shown) is approximately the same as that in Fig. 6.

Single-crystal measurements were made with the scattering vector in the $[11\bar{2}0]$, $[11\bar{2}1]$, and $[0002]$ directions. The long-wavelength side of the experimental Compton line for the outer electrons in two directions is shown in Fig. 7(a) (the calculated $1s^2$ contribution has been subtracted from these data). In Fig. 7(b), the magnitude of the slope of the Compton line for the outer electrons is plotted for the three directions. These results are very similar to those of positron-annihilation experiments (except for the higher-momentum components in the Compton results) and show that the momentum density (and hence the charge density) is flattened along the basal plane.¹⁵ Measurements at the center of the line [$J(0)$] with the scattering vector along the c axis and in the basal plane give $(J(0) \text{ for } [0002]) / (J(0) \text{ for } [11\bar{2}0]) = 1.045 \pm 0.01$. Thus a slice in the basal plane in momentum space (or real space) contains about 4.5% more momentum density (or charge density) than a slice perpendicular to the basal plane in the $[11\bar{2}0]$ direction. This is qualitatively consistent with the known c/a ratio (1.568) being 4% less than that for close packing of spheres (1.63).

The results for the Be core $1s^2$ electrons are particularly puzzling. Figure 8 shows the measured $J(z)$ (for long wavelengths) and $I(p_0)$, as well as the Hartree-Fock free-atom $J(z)$ and $I(p_0)$. [The area of the calculated curves has been normalized according to Eq. (10).] If it is assumed that the core is essentially unchanged

¹⁵ A. T. Stewart, J. B. Shand, J. J. Donaghy, and J. H. Kusmiss, Phys. Rev. **128**, 118 (1962); S. Berko, *ibid.* **128**, 2166 (1962).

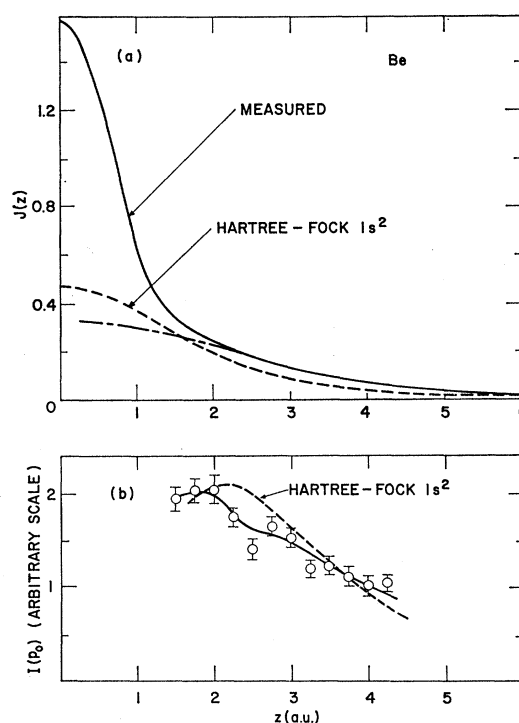


FIG. 8. (a) Measured $J(z)$ (solid curve) and Hartree-Fock $2s^2$ $J(z)$ (dashed curve) for Be. The ratio of the areas under the measured and calculated curves satisfied Eq. (10). An extrapolation of the measured $J(z)$ having the correct core area is also shown. (b) Experimental (solid curve) and Hartree-Fock $1s^2$ (dashed curve) momentum densities determined from the slope of the corresponding $J(z)$.

between the free atom and the solid, the difference between the experimental and calculated curves is too great to be accounted for. Thus it must be concluded that the core in Be metal is not simply free-atom-like. (If, in obtaining the experimental valence-electron curves shown in Figs. 6 and 7, the experimental core contribution shown in Fig. 8 is subtracted from the data, rather than the calculated $1s^2$ free-atom contribution which was used, little change occurs, except that the high-momentum tails become more pronounced.)

B

Measurements were made on crystalline boron. A calculated free-atom $1s^2 2s^2$ momentum density provides a good fit to the experimental momentum density for $z > 2$ a.u. The experimental valence-electron momentum density for B, obtained by subtracting the calculated Hartree-Fock $1s^2$ contribution, is shown in Fig. 9. No sharp discontinuity is evident in $I(p_0)$ after the instrumental resolution has been accounted for. There is a distinct difference between the calculated free-atom $2s^2 2p$ momentum density and the density measured in the solid. As in Be, the valence electrons appear more $2p$ -like than $2s$ -like. The experimental $I(p_0)$ is even more expanded than the calculated free-atom $2p^3$

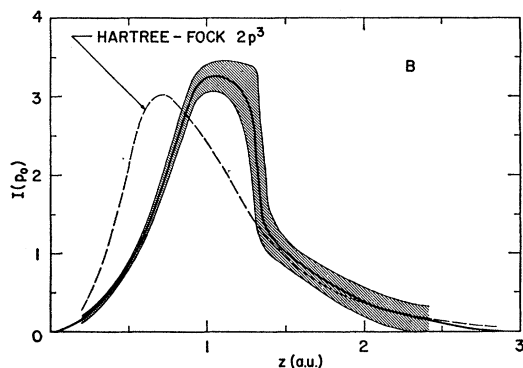


FIG. 9. Measured valence-electron momentum density (corrected for instrumental resolution) and Hartree-Fock $2p^3$ momentum density for B. The Hartree-Fock $1s^2$ core contribution has been subtracted from the measured $J(z)$ to obtain the valence-electron density. The cross-hatched area denotes the experimental uncertainty.

density shown in Fig. 9, a clear demonstration of the effects of bonding.

LiF

The measured Compton line profile $J(z)$ of single-crystal LiF [110] is shown in Fig. 10, together with two calculated Hartree-Fock curves, a superposition of Li^+ and F^- and a superposition of Li^0 and F^0 . The measured $J(z)$ definitely favors the superposition of ionized atoms. (The F $1s$ electrons have a binding energy of ~ 690 eV and make a very small contribution to the long-wavelength side of the line.)

Al and Mg

Figure 11 shows the valence-electron momentum density measured in single-crystal aluminum, obtained by subtracting the calculated $2s^2 2p^6$ free-atom core from the data averaged over the three principal crystallographic directions. The valence electrons appear to be free-electron-like, except for a pronounced high-momentum tail due to correlation effects. The momentum

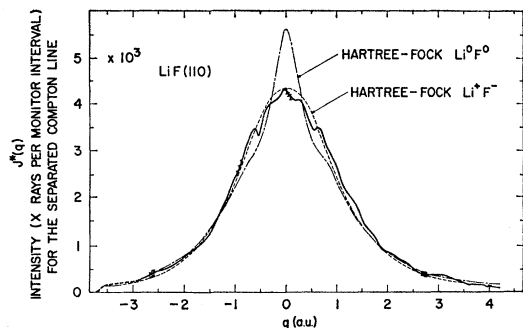


FIG. 10. The $K\alpha_1$ component of the measured Compton line (corrected for instrumental resolution and absorption and with background subtracted) for a LiF crystal with the scattering vector along [110] (solid curve), and the calculated Hartree-Fock $J(z)$ for Li^+F^- [$\text{Li}(1s^2)\text{F}(1s^2 2s^2 2p^6)$] and for Li^0F^0 [$\text{Li}(1s^2 2s)\text{F}(1s^2 2s^2 2p^6)$] (dashed curves).

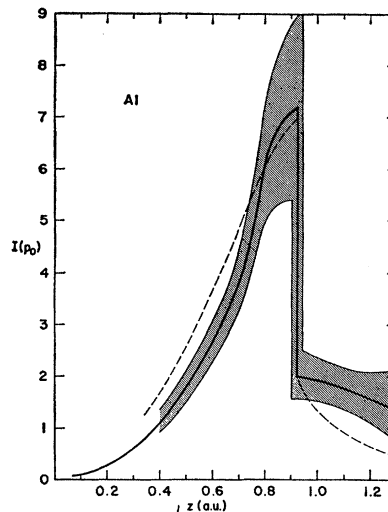


FIG. 11. The Al valence-electron momentum density obtained from the data corrected for instrumental resolution [$J^*(z)$], averaged over the three principal crystallographic directions after subtracting the calculated Hartree-Fock $2s^2 2p^6$ contribution. The experimental uncertainty is shown by the cross-hatched area. The dashed curve is from Ref. 13.

surface is spherical within the experimental uncertainty, although anisotropy is found near $z=0$. Magnesium-single-crystal measurements also show considerable structure near $z=0$. (These details will be studied further with a higher-intensity x-ray source.) As in Li and Na, there is a sharp break in the experimental Compton line (corrected for instrumental resolution) in Al and Mg associated with the Fermi momentum. In both metals the break occurs, within the experimental uncertainty, at the free-electron values, which are 0.926 a.u. in Al and 0.723 a.u. in Mg. In both single and polycrystalline Al the experimental value of p_f is 0.922 ± 0.02 a.u. In Fig. 11, the calculated $I(p_0)$ for the interacting electron gas with parameters appropriate to Al is shown.¹³ The measured correlation effects appear somewhat larger than those given by the calculation. Positron-annihilation results in Al are (1) approximately free-electron-like, with $p_f = 0.95 \pm 0.01$ a.u. (a dependence of p_f on crystal orientation is observed) and (2) essentially devoid of higher momentum components above p_f .

An interesting feature of the Al data is the discrepancy between the measured core-electron momentum density and the calculated Hartree-Fock $2s^2 2p^6$ density, shown in Fig. 12. (The $1s^2$ electrons are not excited.) The measured momentum density for the Al core is more extended in momentum space than that for the free-atom calculation, whereas in Mg the measured core density is in agreement with the calculated free-atom $2s^2 2p^6$ core. Qualitatively, this corresponds to the results of DeMarco for the x-ray scattering factor of Al, which suggest an expansion of the core-electron charge density (in real space), and the results of Weiss

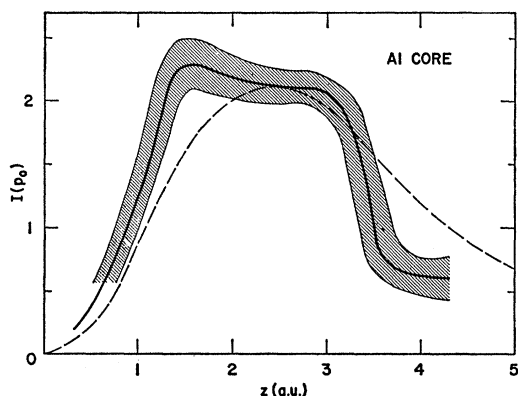


FIG. 12. Measured Al core-electron momentum density and the Hartree-Fock $2s^2 2p^6$ momentum density (dashed curve). For $z < 1.6$ an estimated valence-electron contribution has been subtracted from the measured $J(z)$ to obtain the curve shown. The experimental uncertainty is denoted by the cross-hatched area.

for the x-ray scattering factor of Mg, which show agreement with the calculated free-atom scattering factor.¹⁶

The core-electron momentum densities determined from the Compton-scattering measurements are in agreement with those obtained from Hartree-Fock free-atom calculations in Li, B, Na, and Mg, but not in Be and Al.

TOTAL COMPTON CROSS-SECTION MEASUREMENTS

The measurements reported above are not absolute and, indeed, need not be, except that the separation of core electrons and valence electrons depends partly on the total cross section for each electron group [Eq. (10)]. A separate, absolute measurement of the total Compton cross section was made in the following way. A monochromatic beam of Mo $K\alpha$ x rays [selected by a LiF (200) monochromator] was scattered through 120° in symmetric reflection from a flat sample. The incident beam power I_0 was determined by direct counting, using calibrated absorbers. The scattered power I is given by

$$I = I_0 \left(\frac{e^2}{mc^2} \right)^2 \xi \left(\frac{1 + \cos^2 2\alpha \cos^2 2\theta_c}{1 + \cos^2 2\alpha} \right) \frac{AN}{R^2(\mu + \mu^*)} \times (1 + e^{-(\mu + \mu^*)t/\cos\theta_c}) \int_{-\infty}^{\infty} J(q) dq, \quad (12)$$

where e^2/mc^2 is the classical electron radius, α the Bragg angle of the monochromator, $2\theta_c$ the scattering angle, A/R^2 the solid angle subtended by the detector, N the number of atoms per cm^3 , $\mu + \mu^*$ the linear absorption coefficient of the unmodified and modified

TABLE II. Measured and calculated total Compton cross section ($Z - \mathcal{F}$) for Mo $K\alpha$ scattered 120° ($\sin\theta/\lambda = 1.22 \text{ \AA}^{-1}$), in electron units.

	Calculated	Measured	Valence contribution	Core Contribution
Be	3.91	3.93 ± 0.06	2.00	1.91
Al	11.2	11.2 ± 0.2	3.00	$(2s^2 2p^6) 8.0, (1s^2) 0.2$
LiF	10.95	11.2 ± 0.2	8.00	$(\text{Li} 1s^2) 1.98, (\text{F} 1s^2) 0.97$
Li	2.98	...	1.00	1.98
Na	9.6	...	1.00	$(2s^2 2p^6) 8.0, (1s^2) 0.6$

radiation, t the sample thickness, and ξ the relativistic correction given by

$$\xi = \left\{ 1 + \frac{(h\nu_0/mc^2)^2 (1 - \cos 2\theta_c)^2}{(1 + \cos^2 2\theta_c) [1 + (h\nu_0/mc^2)(1 - \cos 2\theta_c)]} \right\} \times \left(1 + \frac{h\nu_0}{mc^2} (1 - \cos 2\theta_c) \right)^{-3}. \quad (13)$$

Between the sample and the detector was a Y_2O_3 filter (absorption edge at 0.727 \AA) which transmitted the modified radiation but absorbed essentially all of the unmodified radiation. A separate measurement was made to determine the transmission efficiency of the filter over the wavelength range of interest. Thus the total cross section $\int J(q) dq$ could be deduced, since all the other quantities in Eq. (12) could be determined. [A small fraction of the Compton line ($\sim 4\%$) occurs at wavelengths shorter than 0.727 \AA and thus is absorbed by the filter, but this could be calculated with sufficient accuracy from the experimental line shape.] The measured values of the total cross section are given in Table II, along with the calculated cross-section values of Freeman (commonly denoted $Z - \mathcal{F}$).¹⁷ While absolute measurements were not made for Li or Na, the agreement between the measured and calculated values shown in the table provides a justification for using the calculated cross sections in these two metals.

DISCUSSION

These are probably the first Compton line-shape measurements made with sufficient resolution to allow a determination of momentum densities. The principal advantage of this experimental technique is its sensitivity to the valence electrons, and this should provide a good test of band calculations. In addition, the magnitude and position of the discontinuity in the momentum density of metals can be determined from the data.

While the information obtained from the Compton measurements in solids appears promising, it would certainly be desirable to make accurate measurements on a simple system such as an inert gas, in order to further explore problems such as the validity of the

¹⁶ J. J. DeMarco, *Phil. Mag.* **15**, 483 (1967); R. J. Weiss, *ibid.* **16**, 141 (1967).

¹⁷ A. J. Freeman, *Phys. Rev.* **113**, 176 (1959); *Acta Cryst.* **12**, 929 (1959); **13**, 190 (1960).

TABLE III. Values of y versus q for Mo $K\alpha_1$ ($\lambda=0.7093 \text{ \AA}$), $2\theta_c=118^\circ$, for binding energies of 0 and 112 eV.

q (a.u.)	y ($B=0$)	y ($B=112 \text{ eV}$)
-3.50	-5.15	-7.27
-2.00	-2.30	-3.11
-1.00	-1.05	-1.69
0.00	0.00	-0.55
1.00	0.91	0.42
2.00	1.74	1.28
4.00	3.15	2.76
6.00	4.35	4.01
8.00	5.35	5.11

impulse approximation and the accuracy of Hartree-Fock calculations of momentum densities.

The x-ray intensity produced by available x-ray tubes has, to date, limited the Compton measurements to elements below atomic number ~ 15 , because of the competing process of photoelectric absorption. However, there appears to be no technical reason why intensities cannot be increased, so that at least the $3d$ transition metals can be studied.

The momentum density deduced for the core electrons is subject to greater uncertainty than that deduced for the valence electrons, particularly when binding effects are important. Some of the uncertainty can probably be resolved by making measurements with two radiations of appreciably different energy. Corrections to the impulse approximation become important if binding effects are significant. It appears from our data that the impulse approximation breaks down when the energy loss of the photon is less than about twice the binding energy. When the energy loss of the photon is only slightly larger than the binding energy, conservation of energy gives $\hbar\Delta\nu = p^2/2m + B$, where B is the binding energy. In this limit the process is slow enough that the interelectron potentials permit the atom to adjust to the hole being created (a sort of "adiabatic approximation"). For \mathbf{k}_0 and \mathbf{k} fixed, $|p|$ is uniquely determined, since B is fixed. The summation over all final states \mathbf{p} then involves an integration over a sphere of radius $|p|$ (the integration is over a plane in the impulse approximation), and the cross section becomes

$$\frac{d\sigma}{dk} \propto \frac{2\pi}{|\mathbf{k}-\mathbf{k}_0|} \int_{|y|}^{|y|+2p} |\chi(p_0)|^2 p_0 dp_0, \quad (14)$$

$$y = |\mathbf{k}-\mathbf{k}_0| - p = |\mathbf{k}-\mathbf{k}_0| - [2m(\hbar\Delta\nu - B)]^{1/2}.$$

For small q and $B=0$, y (the electron momentum) is again $\sim q$. However, as the binding energy increases, y and q differ appreciably, as shown in Table III for Mo $K\alpha$, $2\theta_c=118^\circ$. The effect produces a large asymmetry in the line shape as well as a shift of the centroid to longer wavelengths. It is clear from our data that the adiabatic approximation is only valid in the immediate vicinity of the binding energy. In Fig. 13, the data for polycrystalline Be has been folded about $z=0$

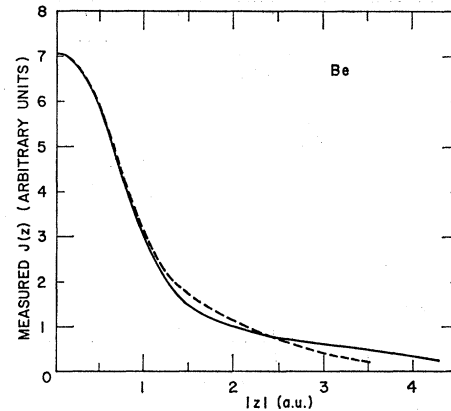


FIG. 13. Measured $K\alpha_1$ component of the Compton line for Be (corrected for absorption and with background subtracted) folded about $z=0$ to show the effects of binding on the core. Dashed curve ($-z$), solid curve ($+z$).

to show the effect of binding on the core-electron Compton profile.

By plotting $p_0^2 I(p_0)$ versus p_0^2 for the valence electrons in a metal, one obtains the density of kinetic-energy states for the band electrons. For most of the standard calculations in solids the potential energy over the band is essentially a slowly varying function of energy, so that the density of kinetic-energy states represents an *approximate ground-state* density of states. When one attempts to obtain density-of-states curves from soft x-ray spectra or from optical data, one uses measurements made in the adiabatic approximation, i.e., measurements made near absorption edges. In these cases, either the initial- or final-state wave functions are excited states, which gives rise to uncertainties when comparing the experimental results with calculations, since the latter are generally concerned only with the ground-state density of states. While our results have the advantage accruing from the impulse approximation, we have not included any such plots here. The reason is simply that the momentum density itself provides a crucial test of band calculations, and little more is gained in the density-of-states representation.

The results presented in this paper should be considered as an initial survey of the potentials of the method. The promise of a significant increase in intensity should enable the resolution in momentum space to be increased from the present ± 0.015 a.u. to better than ± 0.005 a.u.

ACKNOWLEDGMENTS

We wish to thank Dr. R. J. Harrison, Professor S. Berko, Professor A. T. Stewart, Dr. P. M. Platzman, Dr. J. D. Childress, and Dr. J. P. Carbotte for many useful discussions, and Dr. D. R. Chipman for advice during the course of the experiments.